7
Defect Levels Through Hybrid Density Functionals: Insights and Applications

Audrius Alkauskas, Peter Broqvist, and Alfredo Pasquarello

7.1
Introduction

Defects strongly affect properties of materials. For example, doping a semiconductor with a small number of impurity atoms leads to a significant change of its conductivity making such materials useful for technological applications. Similarly, optical transitions involving electronic states of defects can induce a coloration of the otherwise transparent solid, a frequently encountered phenomenon in natural crystals. Also, the mechanical properties and the long-term stability of materials are largely controlled by point and line defects.

It is therefore not suprising that the theoretical study of point defects in solid materials has a long history [1]. Many properties of defects are nowadays well understood. These include for instance the nature of hydrogenic impurities in elemental semiconductors and the energy splittings resulting from local crystal fields. However, these kinds of defects represent just a small class of all possible defects.

Technological developments, particularly in the areas associated to energy and information, lead to the consideration of a vast variety of novel and complex materials. A nonexhaustive list of applications includes solar cells [2], novel metal–oxide–semiconductor field-effect transistors [3], longer-serving batteries [4], solid-state light-emitting diodes [5], and solid fuel cells. The behavior of such devices is generally influenced or governed by a myriad of defects that form in the bulk or at the interfaces between the different materials. Those defects are often *deep*, i.e., they are characterized by localized electronic states which bare little resemblance to the electronic states of the host material and possess ionization energies much larger than typical thermal energies. The experimental characterization of such defects is often very difficult, and thus theoretical studies are not only valuable but also essential. However, because of their deep nature, the theoretical description of the associated electronic states is beyond the reach of simple models. This explains the continuous efforts deployed in the theoretical studies of defects [6].

To study localized defects with deep energy levels, it is necessary to treat the atomic and the electronic structure in a self-consistent way. In the last decades, density

Advanced Calculations for Defects in Materials: Electronic Structure Methods, First Edition.
Edited by Audrius Alkauskas, Peter Deák, Jörg Neugebauer, Alfredo Pasquarello, and Chris G. Van de Walle.

functional theory (DFT) has been the workhorse for such calculations. Since the exchange–correlation energy, a crucial ingredient in the theory, is not available in an exact form, practical calculations generally rely on approximate expressions, such as the local density approximation (LDA) or the generalized gradient approximation (GGA). Though largely successful, these standard approximations to DFT suffer from several shortcomings. The most serious one for the study of defect levels is the infamous "band-gap problem." Band gaps calculated in the LDA and the GGA are significantly smaller than experimental ones. In some cases, a vanishing band gap is obtained for materials which possess a finite one. In the present paper, we mainly focus on formation energies of defects in different charge states and on the associated electronic transition levels. The defect charge state depends on the electron chemical potential, for which the band gap is the relevant energy scale. Therefore, a correct reproduction of the bulk band gap is imperative for achieving a successful theoretical description [7–15].

There exist many methods which go beyond semilocal approximations to DFT and which alleviate the "band-gap problem." Examples of the application of different theoretical methods, some specific to the defect problem, can be found in Refs. [16–35]. In this review article, we focus on hybrid density functionals. These functionals employ the correlation potential from semilocal approximations, but admix a small fraction of nonlocal exchange to the exchange described within the GGA [36–38]. Since band gaps are underestimated with semilocal density functionals and overestimated with full Hartree–Fock exchange, they are naturally improved through the use of hybrid functionals [39, 40]. We here limit the discussion to hybrid functionals based on bare Coulomb exchange. Recently, a variety of hybrid functionals have been proposed, including *screened* nonlocal exchange [41, 42], spatially varying mixing coefficients, and range-separated functionals. For an overview, we refer the reader to Ref. [43].

The present review article is organized as follows. In Section 7.2 we describe the computational toolbox employed in our calculations, and then discuss the quantities that need to be calculated. The hybrid functionals used in the present work are introduced and their performance is discussed. The comparison between defect energy levels calculated with semilocal functionals on the one hand and with hybrid functionals on the other hand provides some fundamental insight into the properties of deep defects. These are presented and discussed in Section 7.3. In order to improve the description of the band gap in hybrid functionals, it has become common practice to adjust the fraction of admixed nonlocal exchange. In Section 7.4, several arguments supporting this empirical procedure are discussed. In Section 7.5 we apply our theoretical scheme to two defect systems and compare our results with available experimental data. Finally, in Section 7.6 we discuss shortcomings and advantages of the proposed scheme, and draw conclusions.

7.2 Computational Toolbox

The calculations in this work were performed within the plane-wave pseudopotential scheme. Defect systems and interfaces are modeled through large supercells. The

ionic cores are described with soft norm-conserving pseudopotentials [44]. Throughout this study, we used a kinetic energy cutoff of 70 Ry, sufficiently high to converge the properties of all the pseudopotentials in this work, including Hf, O, and C. As reference GGA functional, we adopted the functional proposed by Perdew, Burke, and Ernzerhof (PBE) [45]. Pseudopotentials were generated at the PBE level and were used unmodified in calculations with hybrid functionals. Although this is not formally justified, this approach gives a very good description for systems with first-row elements, as can be inferred from comparisons with all-electron calculations [46]. However, for heavier elements this approximation may admittedly involve errors [47]. The Brillouin zone was sampled at the sole Γ-point in most calculations, but denser *k*-point meshes were used when necessary, for example in the determination of accurate band-edge shifts. Further technical details about specific systems are given below. Structural relaxations were carried out at the PBE level. We used the codes CPMD [48, 49] and Quantum-ESPRESSO [50].

7.2.1
Defect Formation Energies and Charge Transition Levels

The principal quantity that needs to be calculated is the formation energy $E_f^{D,q}$ of the defect D in its charge state q as a function of the electron chemical potential E_F [51]:

$$E_f^{D,q}(E_F) = E_{tot}^{D,q} - E_{tot}^{bulk} - \sum_\alpha n_\alpha \mu_\alpha + q(E_V + E_F). \tag{7.1}$$

In this expression $E_{tot}^{D,q}$ is the total energy of the defect system, E_{tot}^{bulk} the total energy of the unperturbed host, n_α the number of extra atoms of species α needed to create the defect D, and μ_α is the corresponding atomic chemical potential. The electron chemical potential is referred to the valence band maximum (VBM) E_V. It varies between zero and the band-gap E_g. Charge transition levels correspond to specific values of the electron chemical potential for which two charge states have equal formation energies. Let us for example consider charge states q and q'. Equating the expressions of the formation energies defined in Eq. (7.1);, we obtain the value for the charge transition level $\varepsilon(q/q')$:

$$\varepsilon(q/q') = \frac{E_{tot}^{D,q} - E_{tot}^{D,q'}}{q' - q} - E_V. \tag{7.2}$$

For example, the charge transition level $\varepsilon(0/+)$ is given via:

$$\varepsilon(0/+) = E_{tot}^{D,0} - E_{tot}^{D,+} - E_V. \tag{7.3}$$

The total energies of charged systems appearing in Eq. (7.1) need to be corrected to speed up the convergence with respect to the supercell size. First, the total energy is corrected by a term $q\Delta V$, ΔV being the potential difference needed to align the potential far from the *neutral* defect to that of the unperturbed bulk. Second, the total energy is corrected for the spurious electrostatic interaction due to the periodic boundary conditions, for which we use the electrostatic correction of Makov and

Payne [52]. These two corrections are always used unless otherwise stated. While the Makov–Payne correction is known to fail in some specific cases, it is generally quite accurate in the case of extremely localized defects. For instance, for defects in SiO_2, the charge transition levels are already converged for moderate supercell sizes (72 atoms) when this electrostatic correction is included. When accurate quantitative results are needed, it is recommended to use either careful extrapolation schemes [53–55] or more elaborate methods for correcting the electrostatic interactions in the supercell [14, 56]. We note that in this respect the present work is mostly concerned with the comparison between results obtained with different functionals, for which the electrostatic corrections are nearly the same and thus do not represent an issue.

Since the electron chemical potential in experiments is generally referred to the VBM, $\varepsilon(q/q')$ defined in Eq. (7.2) is the relevant physical quantity. However, we find useful in Section 7.3 to consider charge transition levels $\bar{\varepsilon}(q/q')$ referred to an appropriately defined average local potential ϕ in the supercell rather than to the VBM:

$$\bar{\varepsilon}(q/q') = \frac{E_{\text{tot}}^{D,q} - E_{\text{tot}}^{D,q'}}{q' - q} - \phi. \tag{7.4}$$

7.2.2 Hybrid Density Functionals

While a number of hybrid functionals have been proposed, we focus in this paper only on one-parameter hybrid functionals based on the bare Coulomb exchange, in which a fraction a of nonlocal exact exchange is admixed to the exchange described within the GGA. By nonlocal exact exchange we here refer to the orbital-dependent expression for exchange appearing in the Hartree–Fock theory [57]. This leads to a generalized Kohn–Sham scheme in which the exchange potential is different for each electronic state the non-local part of which is defined as $\hat{V}_i \psi_i = \partial E_{\text{x}}^{\text{exact}} / \partial \psi_i$. The exchange energy is thus given by

$$E_{\text{x}}^{\text{hybrid}} = a E_{\text{x}}^{\text{exact}} + (1-a) E_{\text{x}}^{\text{GGA}}. \tag{7.5}$$

The correlation potential is usually taken unmodified from the GGA. When the fraction $a = 0.25$ is used together with the PBE approximation for the semilocal part [38], the hybrid functional is referred to as the PBE hybrid. We here use the notation PBE0, but other notations such as PBEh or PBE1PBE are also in use. The value of $a = 0.25$ has been rationalized in case of molecular systems and is considered to be a good compromise for many systems [38]. However, there is no firm theoretical justification for this choice and the optimal mixing coefficient is admittedly system or even property dependent [38, 58].

For many materials, the PBE0 provides an improved description of the energetic and structural properties when compared to the PBE [40, 59]. Lattice constants, formation energies, and bulk moduli of semiconductors and insulators are generally in a better agreement with experimental data [59]. A similar improvement is also

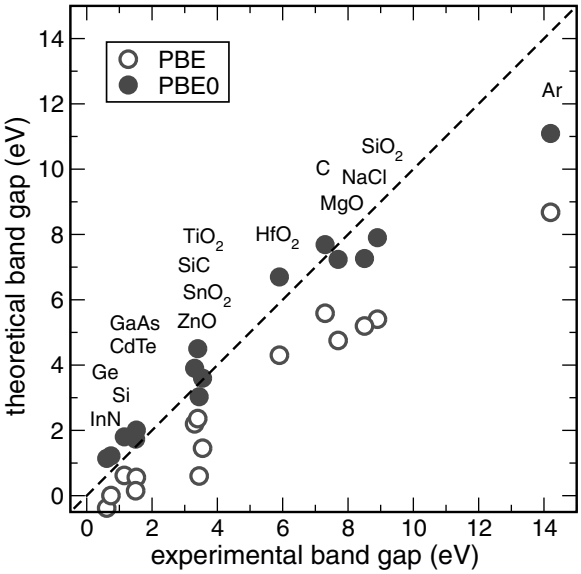

Figure 7.1 (online color at: www.pss-b.com) Calculated versus measured single-particle band gaps for 15 different materials. PBE: open disks, PBE0: filled disks. Results for GaAs, C, MgO, NaCl, and Ar are taken from Ref. [40]; results for InN and ZnO are taken from Ref. [60]; the result for SnO_2 is taken from Ref. [33]; the result for TiO_2 (anatase form) is taken from Ref. [61]; results for Si, SiC (4*H* polytype), HfO_2, CdTe, and SiO_2 are from our calculations.

observed for molecules. However, for metallic systems the use of exact exchange gives rise to unphysical derivative discontinuities at the Fermi level.

Even more importantly than the improvement in structure and energetics, the PBE0 substantially improves the calculated band gaps [40]. This is shown in Figure 7.1. The improvement is especially evident for materials such as Ge or InN which have a vanishing or even negative band gap in semilocal approximations. However, it is also evident that the improvement of the PBE0 over the PBE is not systematic. In the PBE0, band gaps are overestimated for low band-gap materials and underestimated for large band-gap ones. The best agreement is thus for intermediate band-gap materials. It is also clear why the fraction $a = 0.25$ is just a good compromise rather than a universal parameter. In fact for both the PBE and the PBE0 the dependence of the theoretical gap on the experimental one is approximately described by a concave function. For PBE0 ($a = 0.25$), the concave function crosses the diagonal defined by $E_g^{th} = E_g^{expt}$ at about 5 eV. Hence, the theoretical band gaps are overestimated for some materials and underestimated for others. This behavior applies to hybrid functionals with any other reasonable mixing coefficient a.

7.2.2.1 **Integrable Divergence**

In calculations based on plane-wave basis sets and periodic boundary conditions, exact exchange poses one more challenge due to the long-range nature of the Coulomb interaction. In Fourier space this interaction is proportional to $1/q^2$, and

thus diverges at small q. The singularity is integrable, but its straightforward calculation would require very dense k-point meshes. Gygi and Baldereschi [62] proposed a method to treat this singularity. In the matrix element of the exchange operator, they normalized the integrand by substracting an auxiliary function which admits an analytical integration over the Brillouin zone. This method is suitable to be adapted to much sparser k-point samplings, including those limited to the sole Γ-point [46]. The effect of the singularity of the exchange potential can be cast into a correction to the $\boldsymbol{G} = 0$ term of the potential [46, 63]. The Fourrier transform $\Phi(\boldsymbol{G})$ of the exchange interaction is then given by

$$\Phi(\boldsymbol{G}) = \begin{cases} \dfrac{1}{\Omega}\dfrac{4\pi}{G^2} & \text{for} \quad \boldsymbol{G} \neq 0, \\ \chi & \text{for} \quad \boldsymbol{G} = 0, \end{cases} \tag{7.6}$$

where Ω is the volume of the supercell and the singularity correction χ is expressed as

$$\chi = \lim_{\gamma \to 0} \left[\frac{1}{\sqrt{\pi\gamma}} - \frac{4\pi}{\Omega} \sum_{\boldsymbol{G}} \frac{e^{-\gamma G^2}}{G^2} \right]. \tag{7.7}$$

The total energy of a system of N_{el} electrons is thus corrected by a term $-a\chi N_{el}/2$, where a is the fraction of exact exchange used in the hybrid functional. In Figure 7.2, we give the total energies of Si and SiO_2 as a function of the supercell size and/or the density of the k-point mesh for both PBE and PBE0 functionals [46]. In the latter case, the total energies are given with and without the singularity correction. When

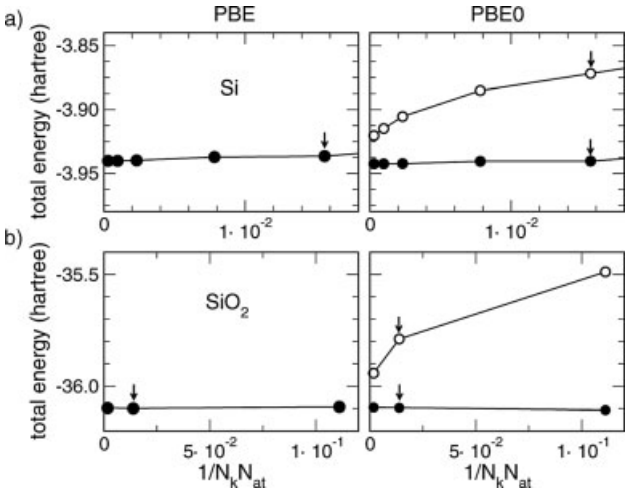

Figure 7.2 Total energies of (a) Si and (b) α-quartz SiO_2 per formula unit versus $1/N_kN_{at}$, where N_k is the total number of k-points and N_{at} the total number of atoms in the supercell. Results obtained in the PBE and the PBE0 are reported in left and right panels, respectively. For PBE0, closed and open symbols indicate values obtained with the singularity correction turned on and off, respectively. Arrows show data points which were also obtained with Γ-point sampling.

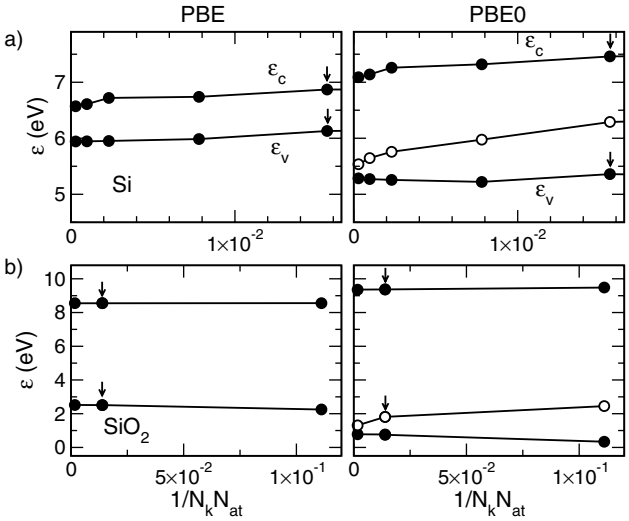

Figure 7.3 Eigenvalues corresponding to the valence (ε_v) and conduction (ε_c) band edges of (a) Si and (b) α-quartz SiO_2 versus $1/N_kN_{at}$, where N_k is the total number of k-points and N_{at} the total number of atoms in the supercell. Results obtained in the PBE and the PBE0 are reported in left and right panels, respectively. For PBE0, closed and open symbols indicate values obtained with the singularity correction turned on and off, respectively. Arrows show data points which were also obtained with Γ-point sampling. The energies obtained with the two functionals are aligned through the average electrostatic potential (*cf.* Ref. [13]).

the correction is included, the convergence properties of PBE0 calculations closely resemble those of PBE calculations. Without the singularity correction the convergence properties clearly deteriorate.

The singularity correction also affects the single-particle eigenvalues. Eigenvalues of unoccupied states remain unchanged, while those of occupied ones shift by $-a\chi$. This is demonstrated in Figure 7.3 for the cases of Si and SiO_2. When the singularity correction is included, hybrid-functional calculations converge as fast as those based on semilocal functionals. This equally holds for calculations with k-point samplings restricted to the Γ-point. Singularity corrections apply equivalently to both delocalized bulk-like states and localized defect or molecular states [46].

Furthermore, singularity corrections are particularly useful in the case of elongated supercells, which may otherwise show an unphysical convergence behavior [46]. Even in the case of screened hybrid functionals which do not show any formal singularity, an analogous treatment of the $q = 0$ limit may lead to a speed up of the convergence with k-point sampling [46].

7.3
General Results from Hybrid Functional Calculations

As shown above, hybrid functionals containing a fixed fraction of exact exchange, such as the PBE0 functional, do not bring theoretical band gaps in agreement with

experimental ones for all materials. Thus, while their straightforward application to the determination of defect levels is expected to lead to an improvement with respect to semilocal functionals, the comparison with experiment remains ambiguous. Nevertheless, we can gain insight into how calculated and measured defect levels should be compared by performing a comparative study between defect energy levels calculated with semilocal and hybrid density functionals. Such a study is expected to reveal how defect levels shift as the description of the band gap improves [13, 64, 65].

To this end, we find useful to refer charge transition levels calculated with different functionals to a common reference potential ϕ. We denote such charge transition levels by $\tilde{\varepsilon}(q/q')$ (*cf.* Eq. 7.4). In our pseudopotential supercell approach, ϕ is obtained from the supercell average of the sum of the local pseudopotential and of the Hartree potential. We argue in the following that this alignment is a convenient choice for determining energy-level shifts induced by the hybrid functional with respect to a reference semilocal calculation.

7.3.1
Alignment of Bulk Band Structures

In this section, we focus on the alignment of bulk band structures obtained with semilocal and hybrid functionals. To simplify the reasoning, let us assume that the same supercell parameters and the same pseudopotentials are used in the two calculations [66]. In this case, the pseudopotential contribution to ϕ is the same in the two calculations, and the adopted alignment consists in aligning the average electrostatic potential in the two theoretical schemes. This alignment allows one to position band edges in the hybrid calculation with respect to those in the semilocal one, i.e., to determine the shift of the VBM ΔE_V and the conduction band minimum (CBM) ΔE_C on a common energy scale, as shown in Figure 7.4.

To analyze the significance of the adopted alignment scheme, it is convenient to conceptually refer to the band offset at the interface between two materials, *A* and *B*. The band offset is a well-defined physical property that can be measured. Following the scheme introduced by Van de Walle and Martin [67], band offsets can be determined by three calculations, namely an interface calculation from which one extracts the line-up of the local average electrostatic potential across the interface and two bulk calculations of materials *A* and *B* which allow one to locate the band edges with respect to the respective average electrostatic potential in each material. This procedure can separately be carried out for the semilocal and for the hybrid scheme.

Alternatively but equivalently, the band alignment in the hybrid scheme can also be obtained from the alignment in the semilocal scheme by the consideration of three sources of difference. By comparing the charge densities in the interface calculations performed at the semilocal and hybrid levels, one can extract the difference in line-up of the average electrostatic potential. Such a difference directly results from the dipoles associated to the difference between the charge densities in the semilocal and in the hybrid schemes. The two other sources of difference can be achieved by separately comparing semilocal and hybrid calculations for bulk materials *A* and *B*. The required differences correspond precisely to the shifts undergone by the band

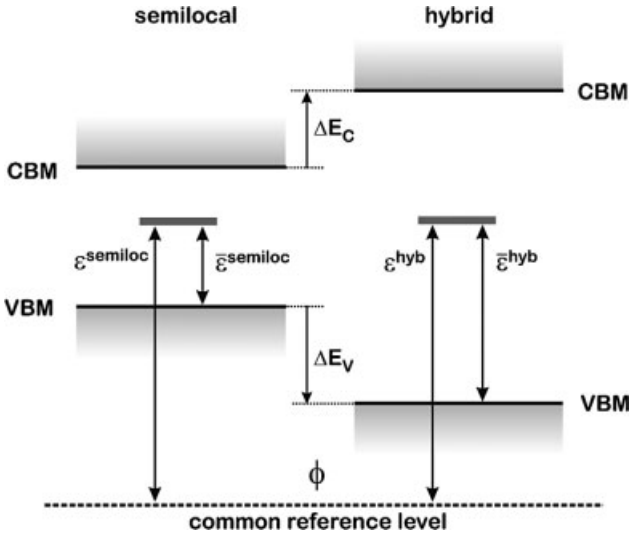

Figure 7.4 (online color at: www.pss-b.com) Charge transition levels calculated within a semilocal and a hybrid functional scheme, aligned to a common reference level ϕ. ε is the charge transition level referred to the respective VBM (Eq. 7.2), $\bar{\varepsilon}$ is the charge transition level referred to the level ϕ (Eq. 7.4). ΔE_V and ΔE_C are the shifts of the VBM and of the CBM in the hybrid-functional calculation with respect to the respective edges in the semilocal calculation. Adapted from Ref. [13].

edges when aligned with respect to the average electrostatic potential. This reasoning thus illustrates that the band offsets in the hybrid scheme would be obtained by combining information that can only be extracted from charge density variations as derived from interface calculations with information that can be derived by aligning the energy scales of periodic bulk calculations as proposed.

In the particular case in which material *B* is the vacuum, we are concerned with a surface system. In this case, it is more natural to adopt the vacuum level at a large distance from the interface as the common reference level for the semilocal and hybrid calculations. From the reasoning in the previous paragraph, it appears clearly that this alignment scheme is not equivalent to the one proposed in this work. Indeed, the alignment to the vacuum level explicitly includes the consideration of a surface and correspondingly charge density differences between the two theoretical schemes might lead to different line-up terms, which would in turn determine a different alignment. Hence, we stress once again that the alignment adopted here is conceptually particularly convenient because it highlights effects of the different theoretical formulations as they result from bulk calculations, without the need for an explicit treatment of interface or surface systems. However, the connection with measurable properties such as work functions and band offsets cannot be made unless such an explicit treatment is considered.

When the charge density is invariant in the two theoretical schemes under comparison, the difference in line-up term vanishes and relative shifts in the

presence of an aligned electrostatic potential also acquire direct physical significance. In practical calculations involving semilocal and hybrid calculations, this condition is very close to being satisfied, as demonstrated for both interface [68] and surface systems [69]. In such cases, the relative band-edge shifts determined through an alignment of the average electrostatic potential give the dominant contribution to the variations undergone by the band offsets [68]. In the case of invariant charge densities, the alignment with respect to the average electrostatic potential is fully equivalent to the alignment with respect to a an external vacuum level achieved through the consideration of a surface.

7.3.2
Alignment of Defect Levels

Once the bulk band structures in the two theories are aligned as described in Section 7.3.1, the alignment of charge transition levels is trivial. This is shown in Figure 7.4. Hitherto, the common reference ϕ was taken to be the average electrostatic potential, but it can for convenience be shifted to coincide with the VBM in the hybrid calculation. In this case $\bar{\varepsilon}^{\mathrm{hyb}}(q/q') = \varepsilon^{\mathrm{hyb}}(q/q')$, and $\bar{\varepsilon}^{\mathrm{semiloc}}(q/q') = \varepsilon^{\mathrm{semiloc}}(q/q') + \Delta E_{\mathrm{V}}$, ΔE_{V} being the shift of the valence band in the hybrid calculation with respect to that in the semilocal one.

In Figure 7.5, we compare charge transition levels $\bar{\varepsilon}(q/q')$ calculated with a semilocal functional (PBE) with corresponding ones obtained with a hybrid functional (PBE0) for a large set of deep defects in four different materials [13]. The chosen materials show band gaps covering a wide range of values: Si (with an experimental band gap of 1.17 eV), 4*H*–SiC (3.3 eV), monoclinic HfO_2 (5.75 eV), and α-quartz SiO_2 (8.9 eV).

Let us first focus on the defects in SiO_2 [64]. Due to the very different band gap of SiO_2 in PBE (5.4 eV) and in PBE0 (7.9 eV), charge transition levels referred to the respective valence band maxima differ significantly. At variance, when the charge transition levels of these defects are referred to the average electrostatic potential, they are very close in the two theoretical schemes. The mean deviation from the ideal alignment is only 0.14 eV. This value is only indicative since it depends on the adopted set of defects. Nevertheless, the alignment of charge transition levels is surprisingly good over a large range of energies. The same alignment property approximately also holds for other materials. For example, in HfO_2 the defect set includes oxygen vacancies and interstitials and the correspondence is similarly very good, with mean deviation of 0.16 eV. The departure from the ideal alignment $[\bar{\varepsilon}^{\mathrm{hyb}}(q/q') = \bar{\varepsilon}^{\mathrm{semiloc}}(q/q')]$ is only slightly larger in SiC and in Si, with a mean deviation of 0.19 eV in both cases.

A detailed inspection reveals that defect levels in the upper part of the band gap tend to shift upwards while those in the lower part tend to shift downwards as the band gap is opened. It was found numerically that the deterioration from the ideal alignment correlates with the increase of the average spread of defect wave functions [13]. In this respect, SiO_2 is an optimal case, because the defect states in this material are characterized by very localized wave functions.

These results can be understood by drawing an analogy between charge transition levels of defect states and ionization potentials or electron affinities of atoms and molecules [13]. The latter quantities can be expressed as total-energy differences and are already well described in semilocal approximations [70, 71], as demonstrated by extensive quantum chemistry calculations [72]. Typical mean deviations of about 0.2 eV are found between calculated and experimental results. Through the use of the Slater–Janak transition-state theory [73, 74], the total energy difference appearing in Eq. (7.4), i.e., $E_{\mathrm{tot}}^{D,q} - E_{\mathrm{tot}}^{D,q'}$, can be related to a matrix element of the defect state at half occupation, which can then be rationalized to carry the same properties as atomic or molecular states insofar its wave function is sufficiently localized [13, 64]. The ideal alignment $\bar{\varepsilon}^{\mathrm{hyb}}(q/q') \approx \bar{\varepsilon}^{\mathrm{semiloc}}(q/q')$ is therefore expected to hold best for atomically localized defects and to deteriorate with the extension of the defect wave function.

The correspondence between energy levels in semilocal and hybrid functional schemes does not hold for single-particle eigenvalues of *extended* bulk-like states, as can be inferred from Figure 7.5 for various materials. We stress that this effect should be explained by invoking the delocalized nature of these states rather than a different behavior of eigenvalues and total-energy differences. In fact, the energy of the VBM E_{V} (and likewise for E_{C}), appearing in the definition of the charge transition level in

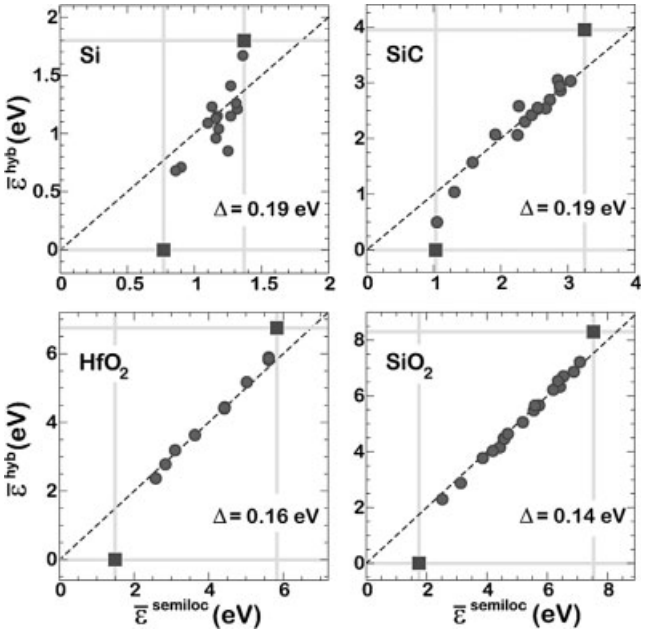

Figure 7.5 (online color at: www.pss-b.com) Comparison between charge transition levels calculated with a semilocal ($\bar{\varepsilon}^{\mathrm{semiloc}}$) and a hybrid ($\bar{\varepsilon}^{\mathrm{hyb}}$) functional for a variety of defects in Si, SiC, HfO_2, and SiO_2. The energy levels corresponding to the VBM and CBM are also shown (squares). All energies are referred to a common reference level ϕ (see text), shifted to coincide with the VBM in the hybrid scheme for convenience. For each material, Δ is the r.m.s. error with respect to the ideal alignment (dashed). Adapted from Ref. [13].

Eq. (7.2), can also be expressed through a total-energy difference: $E_V = E_{tot}^{bulk,0} - E_{tot}^{bulk,+}$. However, for delocalized states, in sharp contrast to localized ones, this total-energy difference is subject to large variations when calculated in semilocal and hybrid functional schemes, reflecting the effect of the "band-gap problem" in the same way as single-particle eigenvalues do. This is the main reason why defect charge transition levels in different theoretical schemes differ so much when referred to their respective valence band maxima.

The use of the unknown exact functional [75, 76] would in either case lead to a correct description of the total energies of localized and extended states. The different description of localized and extended states can be related to specific properties of the approximate functional adopted [70, 71, 77, 78]. The success of approximate functionals in describing total energies of localized systems is related to their fulfillment of the sum rule for the exchange–correlation hole [70]. This stringent criterion is fulfilled at integer electron numbers, yielding accurate total energy differences in calculations for atomic and molecular systems [72]. However, such approximate energy functionals fail in reproducing the linear behavior of the exact functional for fractional electron numbers [75, 76]. As has recently been shown by Mori-Sánchez et al. [78], this failure is at the origin of the incorrect description of single-particle eigenvalues and total energies of delocalized systems. Thereby, these theoretical results establish a clear relation between the "band-gap problem" of approximate density functionals and the delocalized or localized nature of electronic states [78]. Over which length scales the transition takes place between localized and delocalized states is at present still a matter of debate. For an interesting discussion on this issue, we refer to Ref. [71].

The results of this section have provided useful indications concerning the way the "band-gap problem" affects energy levels of deep defects. Defects localized on an atomic scale appear to be already well described at the semilocal level when referred to the average electrostatic potential. In particular, this implies that energy separations between such defect levels are accurately described at the semilocal level and barely affected by the "band-gap problem." The calculations indicate that when the defect state becomes more extended this ideal alignment tends to deteriorate. The shortcoming due to the "band-gap problem" only affects delocalized states such as the valence and conduction band edges. While this of course hinders the correct location of defect levels within the band gap, it nevertheless provides significant insight into the way corrections should be made.

7.3.3
Effect of Alignment on Defect Formation Energies

The fact that charge transition levels of deep defects calculated at different levels of theory tend to be aligned when referred to the average electrostatic potential has important implications for the formation energies of charged defects.

In Figure 7.6, we give a diagram which schematically shows the formation energies of a defect in the positive and the neutral charge state as a function of the electron chemical potential, when calculated with a semilocal (dashed lines) or with a hybrid

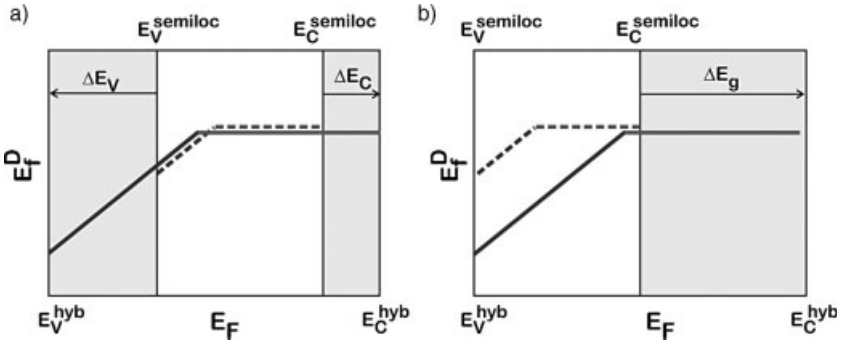

Figure 7.6 (online color at: www.pss-b.com) Formation energies of a point defect as a function of the electron chemical potential E_F calculated with a semilocal (dashed lines) and with a hybrid functional (solid lines). The positive and neutral charge states of the defect are considered. (a) The semilocal and the hybrid calculations are aligned through the average electrostatic potential as in Fig. 7.4; ΔE_V and ΔE_C are the corresponding shifts in the VBM and in the CBM. (b) The VBM of the two calculations are aligned; ΔE_g is the band-gap underestimation in the semilocal calculation with respect to the hybrid one.

(solid lines) functional. The formation energy of a positively charged defect has a positive slope, while that of a neutral defect has a zero slope. The charge transition level corresponds to the value of the electron chemical potential at which the two charge states have equal formation energies. In Figure 7.6a, the transition levels in the two approaches are aligned with respect to the average electrostatic potential as discussed in Section 7.3.1. Let us assume that for the specific defect in Figure 7.6 the charge transition levels in the two theories are indeed very close when referred to the average electrostatic potential. The formation energy of the neutral defect does not depend on the electron chemical potential and we here additionally assume that this energy is quite similar when calculated with semilocal and hybrid functionals. Consequently, this also implies that the formation energies of the positively charged defect are also similar in the two calculations, provided they are taken at the same value of the electron chemical potential referred to the average electrostatic potential. However, since the position of the VBM is different in the two theoretical approaches, the formation energies of the positively charged defect are different when the electron chemical potential is referred to the respective VBM. Thus this clearly illustrates that when the electron chemical potential is found at the VBM as, e.g., for a p-type material, the formation energy of the positively charge defect depends on the location of the VBM relative to the average electrostatic potential. The position of band edges with respect to the average electrostatic potential will be discussed in the next section.

For comparison, we also discuss an alternative alignment scheme which has often been adopted in the literature and which consists in aligning the VBM in the two theoretical approaches, as schematically shown in Figure 7.6b. This alignment scheme assumes that the band-gap problem originates from the wrong placement of the CBM. With this alignment, the charge transition levels are no longer aligned,

and the formation energies of the positively charged defect differ for any value of the electron chemical potential. Under the assumption that the VBM are aligned, it appears contradictory that two theoretical approaches that bear similar total energies for the neutral state would instead differ systematically for the positive charge state, especially when such a charge state results from the absence of electrons in the defect state.

7.3.4 "**The Band-Edge Problem**"

In this section, we elaborate on the "band-gap problem" in relation with the determination of defect levels and argue that it is more appropriate to refer to a "band-edge problem." For this purpose, let us consider two different theories, I and II, which both yield a theoretical band gap in agreement with the experimental one, but different positions of band edges when referred to the average electrostatic potential, as schematically shown in Figure 7.7. For illustration, we consider three kinds of defects. The defect of kind (*a*) corresponds to an atomically localized defect, for which the energy level does not undergo a significant shift, in accord with our observations in Section 7.3.2. On the other extreme, defect (*c*) corresponds to a shallow hydrogenic-like impurity which is known to shift with the band edge to which it is tied. We also consider a defect level (*b*) of intermediate extension, which follows the band edges only to a limited extent.

Figure 7.7 clearly illustrates that reproducing the correct band gap is not a sufficient condition to achieve a correct description of defect levels. When calculated defect levels are compared with experimental ones, the VBM and CBM are natural reference levels. Indeed, the charge transition levels of defects (*a*) and (*b*) referred to their respective theoretical VBM are different despite the fact that the two theories correctly reproduce the experimental band gap! This is a direct consequence of the analysis in Section 7.3.2. For the specific case of the oxygen vacancy in ZnO, such considerations explain to a large extent the scatter of calculated charge transition

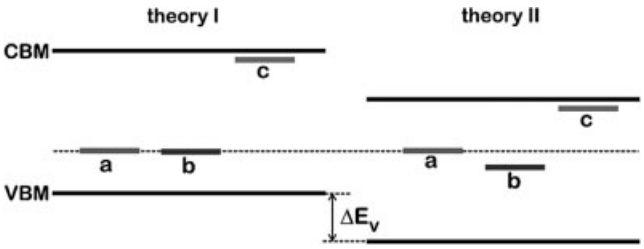

Figure 7.7 (online color at: www.pss-b.com) "The band-edge problem." Comparison of two electronic structure methods, theory I and theory II, for calculations of energy levels of different types of defects: (*a*) an atomically localized defect; (*b*) a defect of intermediate extension; (*c*) a shallow hydrogenic-like defect. The two theories yield the same band gap but different absolute positions of the band edges when referred to the average electrostatic potential. Adapted from Ref. [65].

levels found in the literature [65]. Indeed, different band-gap correction schemes lead to different band-edge positions, while the defect level is generally well defined when referred to the average electrostatic potential [65].

7.4 Hybrid Functionals with Empirically Adjusted Parameters

The comparison of defect charge transition levels calculated with semilocal and hybrid functionals provides insight into the way energy levels of deep defects shift as the description of the band gap improves. The analysis suggests that such defect levels are generally well described at the semilocal level when referred to the average electrostatic potential. Hence, the positioning of the defect levels within the band gap mainly depends on the accuracy by which the adopted functional determines the band edges with respect to this alignment scheme.

As stressed above, a hybrid functional scheme based on the use of a fixed mixing coefficient a does not always yield band gaps in good agreement with experiment. In this section, we address the issue whether band edges determined by hybrid functionals are accurately positioned with respect to the average electrostatic potential, when the mixing coefficient a is tuned to reproduce the experimental band gap. While such an empirical approach is currently in use in the literature, it is ultimately not satisfactory and higher levels of theory will be required to improve the description of the band edges. Nevertheless, the band-gap tuning approach offers a practical scheme in which defect levels are positioned within a band gap of the right value and which can completely be treated within a hybrid functional formulation. It is also based on the well-documented assumption that the structural parameters are generally only moderately affected when the mixing coefficient varies [16, 40, 79], unless the electronic structure itself undergoes important modifications.

As shown in Figure 7.8 for a selected set of materials, semilocal functionals systematically underestimate the experimental band gap. Hybrid functionals generally yield band gaps increasing linearly with the mixing coefficient a [68]. Hence, an optimal mixing coefficient can generally be found for any material:

$$a_{\mathrm{opt}} = \frac{E_{\mathrm{g}}^{\mathrm{expt}} - E_{\mathrm{g}}^{\mathrm{semiloc}}}{\kappa}, \tag{7.8}$$

where $\kappa = \mathrm{d}E_{\mathrm{g}}/\mathrm{d}a$ is the derivative of the band gap with respect to the mixing coefficient. The linear dependence results from the fact that the electron wave functions associated to the band edges do not change significantly with a. Furthermore, this property also signifies that the nature of the band edge states does not change. Indeed, the energy levels of different bands generally behave differently as a varies. Thus, a departure from linearity is expected when the character of the VBM or the CBM changes, as might occur, for example, when sp and d bands cross.

We can provide some support for the tuning of the parameter a by invoking the reasoning of Gygi and Baldereschi [80] in their construction of an approximate GW scheme. Let us consider the nonlocal exchange–correlation potential provided by the

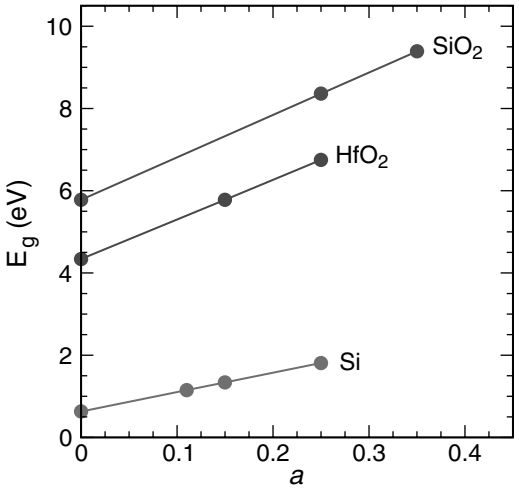

Figure 7.8 (online color at: www.pss-b.com) Dependence of the theoretical band gap on the mixing coefficient a (Eq. 7.5) for several materials. For each material, there is an optimal mixing coefficient a_{opt} for which the hybrid functional reproduces the experimental band gap.

hybrid density functional as a certain approximation to the many-electron exchange–correlation self-energy in the GW approximation, and more particularly to its frequency-independent form, the COHSEX approximation. In this approximation, the long-range interaction is described by screened exchange (SEX), which asymptotically approaches $-1/\varepsilon_\infty(|\boldsymbol{r}-\boldsymbol{r}'|)$. In the hybrid functional formulation, the semilocal part of the exchange–correlation is short-ranged [81] and the long-range part is therefore entirely described by the fraction a of exact exchange: $-a/|\boldsymbol{r}-\boldsymbol{r}'|$. The assumption that the hybrid functional correctly describes the long-range limit, gives the following relation for the optimal mixing coefficient:

$$a_{opt} \approx \frac{1}{\varepsilon_\infty}. \tag{7.9}$$

For metals $\varepsilon_\infty = \infty$, and thus $a_{opt} = 0$, which is a correct and intuitive result. In a metal any fraction of exact exchange would produce unphysical derivative discontinuities (e.g., $\partial\varepsilon_{\boldsymbol{k}}/\partial\boldsymbol{k}$) at the Fermi level. The present discussion is also fully consistent with the reasoning of Fiorentini and Baldereschi [82], who showed that the error in the semilocal band gap approximately scales like $1/\varepsilon_\infty$. Indeed, the smaller the difference between the semilocal and the experimental band gap, the larger the required fraction a_{opt} of exact exchange in the optimal hybrid functional.

In Figure 7.9a, we show the optimal mixing coefficient a_{opt} versus ε_∞ for various materials. Despite some scatter, a clear correlation between a_{opt} and $1/\varepsilon_\infty$ is indeed apparent. The most evident "out-liers," Ge, GaAs, and ZnO, all possess semicore 3d states. This suggests that the long-range screening is not the only property affecting the band gap, and that there is also an effect associated to the s–d coupling [84], which cannot be captured by tuning a to $1/\varepsilon_\infty$. Other reasons for the data scatter are that

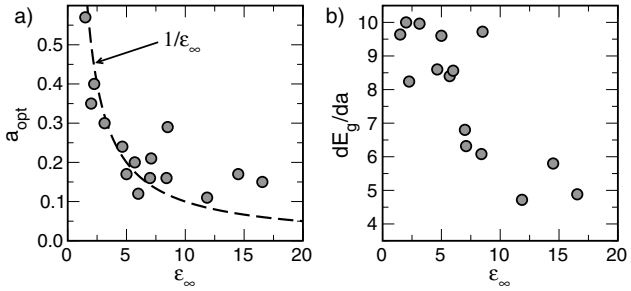

Figure 7.9 (online color at: www.pss-b.com) (a) Optimal mixing coefficients a_{opt} and (b) the derivative of the band gap $\kappa = dE_g/da$ versus the dielectric constant ε_∞ for various materials. The data for the band gaps are taken from the results in Fig. 7.1 and a linear dependence of the band gap on the mixing coefficient a is assumed. For ε_∞, we used experimental data from Ref. [83].

hybrid functionals with $a_{opt} = 1/\varepsilon_\infty$ might inappropriately describe the short-range limit, completely lack the frequency-dependence of the many-body self-energy, and do not account for the anisotropy of the long-range screening when present. Nevertheless, the correlation in Figure 7.9 suggests that the dominant physics is given by the long-range exchange behavior. This is further supported by the good correlation with ε_∞ shown in Figure 7.9b for the quantity $\kappa = dE_g/da$, i.e., the derivative of the band gap with respect to the mixing coefficient. The latter quantity essentially corresponds to $E_g^{HF} - E_g^{semiloc}$, i.e., the difference between the band gap calculated in the Hartree–Fock and in the semilocal scheme.

Once the band gap is tuned to the experimental one, the hybrid functional scheme also provides the shifts of the valence and conduction bands, ΔE_V and ΔE_C. These shifts result from the alignment of the semilocal and hybrid schemes through the average electrostatic potential (*cf.* Section 7.3.1). They indicate to what extent the conduction and valence bands contribute to the band-gap opening. In a hybrid functional formulation, their relative contributions solely depend on the effect of the nonlocal exact exchange operator. The values of these shifts are critical for a correct placement of defect levels within the band gap. The issue that concerns us here is to what extent exact exchange is reliable for the evaluation of such shifts.

In principal, the accuracy of calculated band-edge shifts can be assessed through the consideration of surface systems. Given a well-defined surface structure, the ionization potential and the electron affinity with respect to the vacuum level could be calculated. However, photoemission data for semiconductor and insulator surfaces might be affected by charging effects and by the occurrence of defects and impurities influencing the electrostatics. Therefore, we here prefer to consider band offsets at semiconductor–oxide interfaces, where such electrostatic effects appear better controlled. For a specific interface system, the band offsets can be achieved through the method of Van de Walle and Martin [67]. The band offsets in the hybrid functional scheme can be derived from those in the semilocal scheme through the consideration of the variation of the electrostatic potential offset and through the application of the

Table 7.1 Valence (ΔE_V) and conduction (ΔE_C) band offsets at the Si/SiO_2, SiC/SiO_2, and Si/HfO_2 interfaces calculated in PBE, PBE0, and the mixed scheme (Ref. [68]), in which the mixing coefficient a is different for the two interface components. Experimental band offsets are from Refs. [89, 90] and [91], respectively.

interface		PBE	PBE0	mixed	expt.
Si/SiO_2	ΔE_v	2.5	3.3	4.4	4.4
	ΔE_c	2.3	2.7	3.4	3.4
SiC/SiO_2	ΔE_v	1.4	2.0	3.0	2.9
	ΔE_c	1.7	2.0	2.6	2.7
Si/HfO_2	ΔE_v	2.3	3.1	2.9	2.9
	ΔE_c	1.5	1.9	1.7	1.7

shifts ΔE_V and ΔE_C [68, 85]. On either side of the interface, the theoretical band-gap matches the experimental one by construction. Such a scheme generally requires the use of different a_{opt} for the two bulk components of the interface and is applicable owing to the weak dependence of the interfacial dipole on the mixing parameter a [68]. The comparison between calculated and measured band offsets then provides a sensitive test for the accuracy of band edges as obtained in hybrid functional schemes. In Table 7.1, we present band offsets calculated for three interface model systems: Si/SiO_2 (Refs. [86, 87]), SiC/SiO_2 (Ref. [88]), and Si/HfO_2 (Ref. [28]). When the hybrid functionals are tuned to match the experimental band gaps of the two interface components (*cf.* "mixed" in Table 7.1), the calculated band offsets are found to agree with experiment within only 0.1 eV [89–91]. Despite the limited number of studied systems, the good agreement in Table 7.1 is very encouraging and suggests that hybrid functionals may be relied upon for positioning band edges. This would also imply that nonlocal exchange is the primary cause determining the relative size of band-edge shifts.

Another way of validating the shifts of the band edges obtained from the hybrid functional calculation is through comparison with those calculated with a theory of higher level, such as for instance the *GW* many-body perturbation theory. Recently, Shaltaf *et al.* [92] performed *GW* calculations focusing on such shifts. In Table 7.2, we compare shifts in band edges as obtained with a hybrid functional with those obtained by Shaltaf *et al.* [92] for Si and SiO_2. The band gaps in the hybrid functional calculations with a tuned mixing coefficient are by construction exactly equal to the experimental ones, whereas this is not necessarily the case for the various *GW* approaches. It is therefore more useful to compare relative shifts in the valence and conduction band, i.e., $\Delta E_V/\Delta E_g$ and $\Delta E_C/\Delta E_g$ as obtained in various theoretical schemes. One observes that results obtained with the hybrid functional and with the various *GW* schemes differ by approximately the same amount as the various *GW* schemes differ among themselves. This suggests that the quality of the VBM and CBM shifts provided by the hybrid functional scheme is comparable to that achieved with *GW* methods.

It should be stressed that the study of Shaltaf *et al.* [92] also showed that in *GW* schemes these shifts are more difficult to converge than the band gap, requiring

Table 7.2 Relative shifts of the valence band (ΔE_V) and the conduction band ΔE_C with respect to the change in the band gap ΔE_g for Si and SiO_2, as determined with a hybrid functional (PBE0), a *GW*, and a quasiparticle self-consistent *GW* (QS *GW*) scheme. The latter two results are taken from Ref. [92].

material	quantity	hybrid	*GW*	QS *GW*
Si	$\Delta E_V/\Delta E_g$	−0.54	−0.67	−0.75
	$\Delta E_C/\Delta E_g$	0.46	0.33	0.25
SiO_2	$\Delta E_V/\Delta E_g$	−0.69	−0.56	−0.68
	$\Delta E_C/\Delta E_g$	0.31	0.44	0.32

a very high number of empty states in the calculation of the response functions. Furthermore, these shifts are sensitive to various ingredients of the calculation, such as the plasmon pole approximation, the level of self-consistency of the *GW* approximation, and the vertex corrections [92]. These considerations limit the amount of materials for which such shifts have hitherto been obtained in a reliable way at the *GW* level.

7.5 Representative Case Studies

In this section, we illustrate the application of hybrid functionals to the study of defects through two case studies.

7.5.1 Si Dangling Bond

The first case study concerns the Si dangling bond. This defect corresponds to the atomic structure of the P_b center, which has clearly been observed at interfaces between silicon and its oxide [93]. The dangling bond was modeled by removing four neighboring atoms in a bulk supercell of 216 silicon atoms [29]. Nine of the ten dangling bonds generated in this way were then passivated with H atoms. The core structure of the model is identical to that used in Ref. [23] for modeling the Ge dangling bond.

The relevant charge states of the dangling bond are the positive, the neutral, and the negative charge states. Charge transition levels were calculated in the PBE (the mixing coefficient $a = 0$), the PBE0 ($a = 0.25$), and with a hybrid functional defined by an intermediate mixing coefficient $a = 0.10$. The evolution of the charge transition levels as well as that of the band edges are shown in Figure 7.10a as function of a [29]. The band structures are aligned through the average electrostatic potential. All displayed levels shift linearly with a. The largest shifts are observed for the band edges. The shifts of the charge transition levels $\varepsilon^{+/0}$ and $\varepsilon^{0/-}$ are more moderate, in agreement with general findings [13]. The charge transition levels reported in

Figure 7.10a include the electrostatic Makov–Payne correction. For the present supercell calculation, the application of this correction yields converged values for the charge transition levels [29].

A hybrid functional calculation with a mixing coefficient $a = 0.11$ precisely reproduces the experimental value of the Si band gap, $E_g = 1.17$ eV. For this value of a, we obtained charge transition levels at $\varepsilon^{+/0} = E_V + 0.2$ eV and $\varepsilon^{0/-} = E_V + 0.8$ eV. We compare these values in Figure 7.10b to the experimental density of interfacial traps at the Si–SiO_2 interface as obtained from C/V measurements [93]. The calculated charge transition levels are found to closely correspond to the two experimental peaks at $E_V + 0.26$ eV and $E_V + 0.84$ eV, generally assigned to Si dangling bonds. The good agreement in Figure 7.10b provides support to the practice

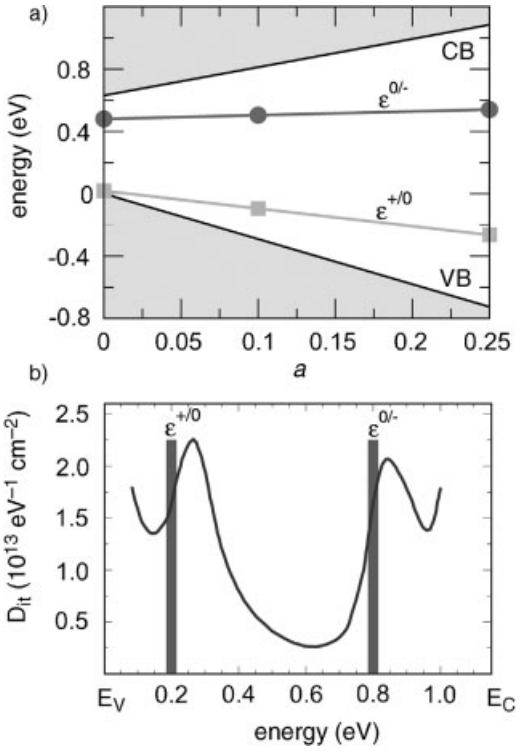

Figure 7.10 (online color at: www.pss-b.com) (a) Dependence of Si band edges and of the charge transition levels $\varepsilon^{+/0}$ and $\varepsilon^{0/-}$ of the Si dangling bond defect on the mixing coefficient a. The vertical energy scale is referred to the VBM in the PBE calculation. Adapted from Ref. [29]. (b) Density of interfacial traps at the Si–SiO_2 as measured by the low-frequency C/V technique in Ref. [93] (solid line). The two pronounced peaks at 0.26 and 0.84 eV originate from P_b defects and correspond to the charge transition levels $\varepsilon^{+/0}$ and $\varepsilon^{0/-}$. The charge transition levels obtained through a hybrid functional calculation with $a = 0.11$ are represented by vertical bars.

of using a mixing coefficient a that brings the theoretical band gap obtained within the hybrid functional scheme in accord with the experimental one.

7.5.2 Charge State of O_2 During Silicon Oxidation

The second case study concerns the charge state of the O_2 molecule during silicon oxidation. The silicon oxidation process has attracted considerable interest because of its key role in the manufacturing of Si-based microelectronic devices. Our present understanding relies to a large extent on the oxidation model proposed by Deal and Grove [94]. In this model, the growth of SiO_2 proceeds by (i) the adsorption of the O_2 molecule on the oxide surface, (ii) the diffusion of molecular O_2 through the bulk-like oxide, and (iii) its subsequent reaction at the semiconductor–oxide interface. Simulation techniques based on DFT have been instrumental for achieving an atomic-scale description of the involved processes [95], such as, e.g., the diffusion mechanism of O_2 in amorphous SiO_2 [96], the oxidation reaction [97], etc. However, one aspect that has long been difficult to address is the charge state of the diffusing oxygen molecule. The difficulty of providing a clear answer to this issue stems from the "band-gap problem" of semilocal approximations to DFT [30, 98].

In bulk SiO_2, the oxygen molecule is stable in the neutral and in the negative charge states [96]. The charge state of the O_2 in the vicinity of the Si/SiO_2 interface is determined by the position of the $(0/-)$ charge transition level with respect to silicon band edges. It is assumed that the molecule is close enough to the interface to allow for charge equilibration with the silicon substrate, yet remaining far from the suboxide region where the oxidation reaction takes place. Thus, the $(0/-)$ charge transition level of the O_2 molecule is first determined in a bulk-like amorphous SiO_2 environment and then positioned with respect to Si band edges through the band alignment at the Si/SiO_2 interface. In Figure 7.11, we show the result of such an alignment procedure as obtained within three different theoretical schemes [30]: (i) the semilocal (PBE) functional; (ii) the hybrid (PBE0) functional; (iii) a mixed scheme, in which the fraction of exact exchange is tuned for each interface component, following the prescription for the calculation of band offsets given above [68].

All three theoretical schemes consistently indicate that the $(0/-)$ charge transition level locates above the Si CBM (Figure 7.11), providing convincing evidence that for electron chemical potentials in the Si band gap the neutral charge state is thermodynamically favored. The three schemes show only small quantitative differences. The separation between the $(0/-)$ charge transition level and the Si CBM is 1.1 eV in the PBE and in the mixed scheme, and reduces to 0.8 eV in the PBE0.

To obtain such a level of qualitative agreement between different theoretical schemes, charge transition levels and band offsets were obtained consistently within each scheme. This should be contrasted with the practice of determining transition levels with respect to the oxide band edges within PBE and using the experimental band offsets for alignment with respect to the Si band edges. Such an alignment procedure implicitly takes the erroneous assumption [68, 92] that the band-gap correction is achieved by the sole displacement of the conduction band. In the case of

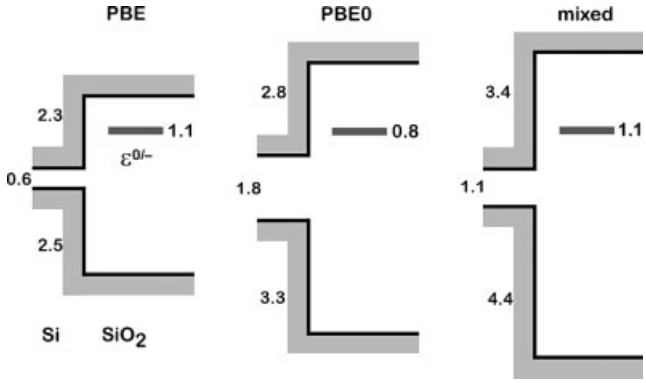

Figure 7.11 (online color at: www.pss-b.com) The alignment of the $(0/-)$ charge transition level of the O_2 molecule at the Si/SiO_2 interface is obtained within three different theoretical schemes: a semilocal functional (PBE), a hybrid functional (PBE0), and the mixed scheme. The Si band gap, the Si/SiO_2 band offsets, and the separation between the defect level and the silicon CBM are given in eV. From Ref. [30].

the O_2 molecule in SiO_2, this approach results in the opposite conclusion that it is the negative charge state which is thermodynamically favored [98].

7.6 Conclusion

Our investigation indicates that hybrid functional schemes offer a viable theoretical tool for determining the location of energy levels of deep defects with respect to the band edges of the bulk material. The issue is conveniently addressed by separately aligning the defect level and the band edges with respect to the average electrostatic potential. In this way, the determination of the defect level can to a large extent be decoupled from the determination of bulk band edges.

As far as the defects are concerned, it appears that their energy levels with respect to the average electrostatic potential are already well described at the semilocal level and that the hybrid-functional description does not lead to any significant modification. In the case of ionization potentials of molecular systems, a similar agreement is recorded and the comparison with experiment shows that an accurate description is achieved. In analogy with the molecular case, this therefore suggests that the energy separation between the defect level and the average electrostatic potential is in many cases already accurately determined at the semilocal and hybrid functional level.

At variance, the position of the band edges is highly sensitive to the fraction of exact exchange considered in the hybrid functional calculation. The use of any fixed fraction of exact exchange does not lead to a systematic improvement of the band-gap description, thereby hindering the use of a hybrid-functional scheme as a predictive tool. It is therefore necessary to resort to an electronic structure method of higher accuracy to identify the position of the band edges. It should be noted that such

a method would be applied in the absence of the defect and could therefore take computational advantage of the full translational symmetry of the host material. This analysis allows us to reformulate the band-gap problem in terms of a band-edge problem, highlighting the importance of a reliable description of bulk bands relative to the average electrostatic potential.

Our work also explored the route of determining band-edge shifts while remaining within the hybrid functional approach. This is done at the cost of empirically adjusting the mixing coefficient a to reproduce the experimental band gap. While such an approach does not offer an ideal solution, several supporting arguments can nevertheless be invoked. In particular, the accuracy of the determined band edges can be assessed either by comparison with electronic-structure theories of higher accuracy or by direct comparison with experimental band offsets. In both cases, available data indicate that the agreement is very encouraging. The present description achieved with hybrid functionals constitutes a noticeable step forward with respect to the case of semilocal functionals in which any conclusion is heavily biased by the band-gap problem.

A generalized use of hybrid functional schemes still requires further work. One important issue is the shift in the band edges with respect to the average electrostatic potential. The validity of shifts determined within hybrid functional schemes should further be investigated by extending the comparison with experiment to a larger set of semiconductor–semiconductor and semiconductor–oxide band offsets. In addition, a more systematic comparison with theoretical schemes of higher accuracy, such as many-body perturbation schemes based on the GW approximation, would be invaluable for further supporting the shifts obtained with hybrid functionals. In particular, such comparisons should also provide insight into whether it is conceptually reasonable to expect that exact exchange dominates the relative value of conduction and valence band shifts.

The use of hybrid functionals with tuned mixing coefficients is clearly unsatisfactory. In the inhomogeneous case of an interface between two materials with very different band gaps, the mixed scheme is advantageous for achieving a good description of band offsets [68]. However, the use of different functionals for the two interface components precludes the study of the transition region and defects therein. Since the optimal mixing coefficients are different on both sides of the interface, a reliable description of the evolution of band edges is not possible with any fixed value of a. Accordingly, the mixing coefficient should depend on the coordinate perpendicular to the interface. This is not practical when plane-wave basis sets are used, but could in principal be achieved in the case of localized basis functions. However, such an approach is conceptually not appealing since the variation across the interface would remain *ad hoc*.

Another problem is related to localized electronic states, such as d and f orbitals, for which self-interaction errors of semilocal density functionals are high. For instance, in many transition metal oxides, such as ZnO, the fraction a required to correctly position the semicore 4s with respect to VBM is not necessarily equal to the value of a reproducing the band gap. This results in a serious deficiency when the role of these d states cannot be neglected. The role of self-interaction errors might be even more

significant in the description of very localized defect states affected by strong polaronic effects, such as Al substitutional to Si in SiO_2 [99, 100], Li substitutional to Zn in ZnO [101–103], the self-trapped hole in NaCl [104], defect-trapped and self-trapped electrons and holes in TiO_2 [105], or the Mg vacancy in MgO [106]. Semilocal density functionals yield excessively delocalized electron densities resulting in inaccurate defect geometries. Hybrid functionals generally improve upon this. However, the mixing coefficient a required for reproducing correct defect geometries can be very different than the value optimizing the band gap [103]. This implies that a single value of a cannot concurrently reproduce the bulk band edges and the ground-state geometries of specific defects. Such an *ad hoc* fixation of the hybrid-functional parameters is clearly disturbing.

In conclusion, hybrid functionals certainly represent a powerful tool for the study of defect levels, but problematic aspects persist requiring great caution in their application. In this work, we restricted the discussion to the class of hybrid functionals based on bare nonlocal exchange, in which the mixing coefficient is allowed to vary. Hybrid functionals based on screened exchange might offer greater flexibility, but it is anticipated that even such functionals would not lead to a universally effective tool when used with fixed parameters [107]. In this context, the approach discussed in this work provides useful insights and guidelines for the theoretical determination of defect levels.

Acknowledgements

We acknowledge useful discussions with J.-F. Binder, A. Carvalho, H.-P. Komsa, A. Janotti, P. Rinke, and C. G. Van de Walle. Financial support from the Swiss National Science Foundation (grant no. 200020-119733/1) is acknowledged. The calculations were performed on computational facilities at DIT-EPFL, CSEA-EPFL, and CSCS.

References

1 Stoneham, A.M. (1975) *Theory of Defects in Solids: Electronic Structure of Defects in Insulators and Semiconductors*, Oxford University Press, Oxford.
2 Green, M. (2003) *Third Generation Photovoltaics: Advanced Solar Energy Conversion*, Springer-Verlag, Berling-Heidelberg.
3 Robertson, J. (2006) *Rep. Prog. Phys.*, **69**, 327.
4 Winter, M. and Brodd, R.J. (2004) *Chem. Rev.*, **104**, 4245.
5 Tsao, J.Y. (2004) *IEEE Circuits Devices*, **20**, 28.
6 Van de Walle, C.G. and Neugebauer, J. (2004) *J. Appl. Phys.*, **95**, 3851.
7 Zhang, S.B., Wei, S.-H., and Zunger, A. (2001) *Phys. Rev. B*, **63**, 075205.
8 Janotti, A. and Van de Walle, C.G. (2005) *Appl. Phys. Lett.*, **87**, 122102.
9 Persson, C., Zhao, Y.-J., Lany, S., and Zunger, A. (2005) *Phys. Rev. B*, **72**, 035211.
10 Janotti, A. and Van de Walle, C.G. (2007) *Phys. Rev. B*, **76**, 165202.
11 Lany, S. and Zunger, A. (2007) *Phys. Rev. Lett.*, **98**, 045501.

12 Zhukovskii, Y.F., Kotomin, E.A., Evarestov, R.A., and Ellis, D.E. (2007) *Int. J. Quantum Chem.*, **107**, 2956.
13 Alkauskas, A., Broqvist, P., and Pasquarello, A. (2008) *Phys. Rev. Lett.*, **101**, 046405.
14 Lany, S. and Zunger, A. (2008) *Phys. Rev. B*, **78**, 235104.
15 Rinke, P., Janotti, A., Scheffler, M., and Van de Walle, C.G. (2009) *Phys. Rev. Lett.*, **102**, 026402.
16 Deák, P., Gali, A., Sólyom, A., Buruzs, A., and Frauenheim, Th. (2005) *J. Phys.: Condens. Matter*, **17**, S2141.
17 Knaup, J.M., Deák, P., Frauenheim, Th., Gali, A., Hajnal, Z., and Choyke, W.J. (2005) *Phys. Rev. B*, **72**, 115323.
18 Lany, S. and Zunger, A. (2006) *J. Appl. Phys.*, **100**, 113725.
19 Hedström, M., Schindlmayr, A., Schwarz, G., and Scheffler, M. (2006) *Phys. Rev. Lett.*, **97**, 226401.
20 Broqvist, P. and Pasquarello, A. (2006) *Appl. Phys. Lett.*, **89**, 262904.
21 Gavartin, J.L., Muñoz Ramo, D., Shluger, A.L., Bersuker, G., and Lee, B.H. (2006) *Appl. Phys. Lett.*, **89**, 082908.
22 Li, J., and Wei, S.-H. (2006) *Phys. Rev. B*, **73**, 041201.
23 Weber, J.R., Janotti, A., Rinke, P., and Van de Walle, C.G. (2007) *Appl. Phys. Lett.*, **91**, 142101.
24 Broqvist, P. and Pasquarello, A. (2007) *Appl. Phys. Lett.*, **90**, 082907.
25 Alkauskas, A. and Pasquarello, A. (2007) *Physica B*, **401/402**, 546.
26 Paudel, T.R. and Lambrecht, R.L. (2008) *Phys. Rev. B*, **77**, 205202.
27 Oba, F., Togo, A., Tanaka, I., Paier, J., and Kresse, G. (2008) *Phys. Rev. B*, **77**, 245202.
28 Broqvist, P., Alkauskas, A., and Pasquarello, A. (2008) *Appl. Phys. Lett.*, **92**, 132911.
29 Broqvist, P., Alkauskas, A., and Pasquarello, A. (2008) *Phys. Rev. B*, **78**, 075203.
30 Alkauskas, A., Broqvist, P., and Pasquarello, A. (2008) *Phys. Rev. B*, **78**, 161305.
31 Stroppa, A. and Kresse, G. (2009) *Phys. Rev. B*, **79**, 201201(R).
32 Broqvist, P., Alkauskas, A., Godet, J., and Pasquarello, A. (2009) *J. Appl. Phys.*, **105**, 061603.
33 Ágoston, P., Albe, K., Nieminen, R.M., and Puska, M.J. (2009) *Phys. Rev. Lett.*, **103**, 245501.
34 Lany, S. and Zunger, A. (2010) *Phys. Rev. B*, **81**, 113201.
35 Deák, P., Aradi, B., Frauenheim, Th., Janzén, E., and Gali, A. (2010) *Phys. Rev. B*, **81**, 153203.
36 Becke, A.D. (1993) *J. Chem. Phys.*, **98**, 1372.
37 Becke, A.D. (1993) *J. Chem. Phys.*, **98**, 5648.
38 Perdew, J.P., Burke, K., and Ernzerhof, M. (1996) *J. Chem. Phys.*, **105**, 9982.
39 Muscat, J., Wander, A., and Harrison, N.M. (2001) *Chem. Phys. Lett.*, **342**, 397.
40 Paier, J., Marsman, M., Hummer, K., Kresse, G., Gerber, I.C., and Ángáyan, J.G. (2006) *J. Chem. Phys.*, **124**, 154709; (2006) *J. Chem. Phys.*, **125**, 249901 (E).
41 Heyd, J., Scuseria, G.E., and Enzerhof, M. (2003) *J. Chem. Phys.*, **118**, 8207; (2006) *J. Chem. Phys.*, **124**, 219906 (E).
42 Krukau, A.V., Vydrov, O.A., Izmaylov, A.F., and Scuseria, G.E. (2006) *J. Chem. Phys.*, **125**, 224106.
43 Janesko, B.G., Henderson, T.M., and Scuseria, G.E. (2009) *Phys. Chem. Chem. Phys.*, **11**, 443.
44 Troullier, N. and Martins, J.L. (1991) *Phys. Rev. B*, **43**, 1993.
45 Perdew, J.P., Burke, K., and Ernzerhof, M. (1996) *Phys. Rev. Lett.*, **77**, 3865.
46 Broqvist, P., Alkauskas, A., and Pasquarello, A. (2009) *Phys. Rev. B*, **80**, 085114; (2010) *Phys. Rev. B*, **81**, 039903.
47 Stroppa, A. and Kresse, G. (2008) *New J. Phys.*, **10**, 063020.
48 Hutter, J. and Curioni, A. (2005) *ChemPhysChem*, **6**, 1788; Car, R. and Parrinello, M. (1985) *Phys. Rev. Lett.*, **55**, 2471; CPMD, Copyright IBM Corp. 1990–2006 Copyright MPI für Festkörperforschung Stuttgart 1997–2001.
49 Todorova, T., Seitsonen, A.P., Hutter, J., Kuo, I. F. W., and Mundy, C.J. (2006) *J. Phys. Chem. B*, **110**, 3685.
50 Giannozzi, P., Baroni, S., Bonini, N., Calandra, M., Car, R., Cavazzoni, C., Ceresoli, D., Chiarotti, G.L., Cococcioni, M., Dabo, I., Dal Corso, A., de Gironcoli, S., Fabris, S., Fratesi, G., Gebauer, R.,

Gerstmann, U., Gougoussis, C., Kokalj, A., Lazzeri, M., Martin-Samos, L., Marzari, N., Mauri, F., Mazzarello, R., Paolini, S., Pasquarello, A., Paulatto, L., Sbraccia, C., Scandolo, S., Sclauzero, G., Seitsonen, A.P., Smogunov, A., Umari, P., and Wentzcovitch, R.M. (2009) *J. Phys.: Condens. Matter*, **21**, 395502, http://www.quantum-espresso.org.

51 Zhang, S.B. and Northrup, J.E. (1991) *Phys. Rev. Lett.*, **67**, 2339.

52 Makov, G. and Payne, M.C. (1995) *Phys. Rev. B*, **51**, 4014.

53 Lento, J., Mozos, J.-L., and Nieminen, R.M. (2002) *J. Phys.: Condens. Matter*, **14**, 2637.

54 Castleton, C.W.M., Höglund, A., and Mirbt, S. (2006) *Phys. Rev. B*, **73**, 035215.

55 Hine, N.D.M., Frensch, K., Foulkes, W. M. C., and Finnis, M.W. (2009) *Phys. Rev. B*, **79**, 024112.

56 Freysoldt, C., Neugebauer, J., and Van de Walle, C.G. (2009) *Phys. Rev. Lett.*, **102**, 016402.

57 Kümmel, S. and Kronik, L. (2008) *Rev. Mod. Phys.*, **80**, 3.

58 Ernzerhof, M., Perdew, J.P., and Burke, K. (1997) *Int. J. Quantum Chem.*, **64**, 285.

59 Paier, J., Hirschl, R., Marsman, M., and Kresse, G. (2005) *J. Chem. Phys.*, **122**, 234102.

60 Fuchs, F., Furthmuller, J., Bechstedt, F., Shishkin, M., and Kresse, G. (2007) *Phys. Rev. B*, **76**, 115109.

61 Labat, F., Baranek, P., Domain, C., Monot, C., and Adamo, C. (2007) *J. Chem. Phys.*, **126**, 154703.

62 Gygi, F. and Baldereschi, A. (1986) *Phys. Rev. B*, **34**, 4405.

63 Carrier, P., Rohra, S., and Görling, A. (2007) *Phys. Rev. B*, **75**, 205126.

64 Alkauskas, A. and Pasquarello, A. (2007) *Physica B*, **401/402**, 670.

65 Alkauskas, A. and Pasquarello, A. unpublished.

66 More complex situations can in principle also be addressed.

67 Van de Walle, C.G. and Martin, R.M. (1987) *Phys. Rev. B*, **35**, 8154.

68 Alkauskas, A., Broqvist, P., Devynck, F., and Pasquarello, A. (2008) *Phys. Rev. Lett.*, **101**, 106802.

69 Lyons, J.L., Janotti, A., and Van de Walle, C.G. (2009) *Phys. Rev. B*, **80**, 205113.

70 Perdew, J.P. and Levy, M. (1997) *Phys. Rev. B*, **56**, 16021.

71 Öğüt, S., Chelikowsky, J.R., and Louie, S.G. (1998) *Phys. Rev. Lett.*, **80**, 3162; Godby, R.W., and White, I.D. (1998) *Phys. Rev. Lett.*, **80**, 3161.

72 Curtiss, L.A., Redfern, P.C., Raghavachari, K., and Pople, J.A. (1997) *J. Chem. Phys.*, **106**, 1063; (1998) *J. Chem. Phys.*, **109**, 42.

73 Slater, J.C. (1972) *Adv. Quantum Chem.*, **6**, 1.

74 Janak, J.F. (1978) *Phys. Rev. B*, **18**, 7165.

75 Perdew, J.P., Parr, R.G., Levy, M., and Balduz, J.L. (1982) *Phys. Rev. Lett.*, **49**, 1691.

76 Perdew, J.P. and Levy, M. (1983) *Phys. Rev. Lett.*, **51**, 1884.

77 Vydrov, O.A., Scuseria, G.E., and Perdew, J.P. (2007) *J. Chem. Phys.*, **126**, 154109.

78 Mori-Sánchez, P., Cohen, A.J., and Yang, W. (2008) *Phys. Rev. Lett.*, **100**, 146401.

79 Heyd, J., Peralta, J.E., Scuseria, G.E., and Martin, R.L. (2005) *J. Chem. Phys.*, **123**, 174101.

80 Gygi, F. and Baldereschi, A. (1989) *Phys. Rev. Lett.*, **62**, 2160.

81 Sham, L.J. and Kohn, W. (1966) *Phys. Rev.*, **145**, 561.

82 Fiorentini, V. and Baldereschi, A. (1995) *Phys. Rev. B*, **51**, 17196.

83 Landolt-Börnstein database, http://www.springermaterials.com.

84 Persson, C. and Zunger, A. (2003) *Phys. Rev. B*, **68**, 073205.

85 Broqvist, P., Binder, J.F., and Pasquarello, A. (2009) *Appl. Phys. Lett.*, **94**, 141911.

86 Sarnthein, J., Pasquarello, A., and Car, R. (1995) *Phys. Rev. Lett.*, **74**, 4682; (1995) *Phys. Rev. B*, **52**, 12690.

87 Giustino, F. and Pasquarello, A. (2005) *Phys. Rev. Lett.*, **95**, 187402; Bongiorno, A., Pasquarello, A., Hybertsen, M.S., and Feldman, L.C. (2003) *Phys. Rev. Lett.*, **90**, 186101; Bongiorno, A., and Pasquarello, A. (2003) *Appl. Phys. Lett.*, **83**, 1417.

88 Devynck, F., Giustino, F., Broqvist, P., and Pasquarello, A. (2007) *Phys. Rev. B*, **76**, 075351.

89 Himpsel, F.J., McFeely, F.R., Teleb-Ibrahimi, A., Yarmoff, J.A., and

Hollinger, G. (1988) *Phys. Rev. B*, **38**, 6084; Keister, J.W., Rowe, J.E., Kolodziej, J.J., Niimi, H., Madey, T.E., and Lucovsky, G. (1999) *J. Vac. Sci. Technol. B*, **17**, 1831.

90 Afanas'ev, V.V., Ciobanu, F., Dimitrijev, S., Pensl, G., and Stesmans, A. (2004) *J. Phys.: Condens. Matter*, **14**, S1839.

91 Oshima, M., Toyoda, S., Okumura, T., Okabayashi, J., Kumigashira, H., Ono, K., Niwa, M., Usuda, K., and Hirashita, N. (2003) *Appl. Phys. Lett.*, **83**, 2172; Renault, O., Barrett, N.T., Samour, D., and Quiais-Marthon, S. (2004) *Surf. Sci.*, **566–568**, 526.

92 Shaltaf, R., Rignanese, G.-M., Gonze, X., Giustino, F., and Pasquarello, A. (2008) *Phys. Rev. Lett.*, **100**, 186401.

93 Poindexter, E.H., Gerardi, G.J., Rueckel, M.-E., Caplan, P.J., Johnson, N.M., and Biegelsen, D.K. (1984) *J. Appl. Phys.*, **56**, 2844.

94 Deal, B.E. and Grove, A.S. (1965) *J. Appl. Phys.*, **36**, 3770.

95 Bongiorno, A. and Pasquarello, A. (2005) *J. Phys.: Condens. Matter*, **17**, S2051.

96 Bongiorno, A. and Pasquarello, A. (2002) *Phys. Rev. Lett.*, **88**, 125901; (2004) *Phys. Rev. B*, **70**, 195312.

97 Bongiorno, A. and Pasquarello, A. (2004) *Phys. Rev. Lett.*, **93**, 086102.

98 Stoneham, A.M., Szymanski, M.A. and Shluger, A.L. (2001) *Phys. Rev. B*, **63**, 241304; Szymanski, M.A., Stoneham, A.M., Shluger, A. (2001) *Solid-State Electron.*, **45**, 1233.

99 Pacchioni, G., Frigoli, F., Ricci, D., and Weil, J.A. (2000) *Phys. Rev. B*, **63**, 054102.

100 Laegsgaard, J. and Stokbro, K. (2001) *Phys. Rev. Lett.*, **86**, 2834.

101 Lany, S. and Zunger, A. (2009) *Phys. Rev. B*, **80**, 085202.

102 Du, M.-H. and Zhang, S.B. (2009) *Phys. Rev. B*, **80**, 115217.

103 Carvalho, A., Alkauskas, A., Pasquarello, A., Tagantsev, A., and Setter, N. (2009) *Phys. Rev. B*, **80**, 195205; (2009) *Physica B*, **23–24**, 4797.

104 Gavartin, J.L., Sushko, P.V., and Shluger, A.L. (2003) *Phys. Rev. B*, **67**, 035108.

105 Morgan, B.J., and Watson, G.W. (2009) *Phys. Rev. B*, **80**, 233102.

106 Droghetti, A., Pemmaraju, C.D., and Sanvito, S. (2010) *Phys. Rev. B*, **81**, 092403.

107 Komsa, H.-P., Broqvist, P., and Pasquarello, A. (2010) *Phys. Rev. B*, **81**, 205118.